APPLICATION OF DYNAMIC SUBGRID G-EQUATION MODEL TO LES OF TURBULENT PREMIXED FLAME OVER BACKWARD FACING STEP

Namseob Park
Hyundai Motor Company
772-1, Changduk-Ri, Namyang-Myun, Whasung-Gun, Kyunggi-Do, 445-706, Korea
namseob@hyundai-motor.com

Toshio Kobayashi
Institute of Industrial Science, University of Tokyo
4-6-1 Komaba, Meguro-ku, Tokyo 153-8505, Japan
kobaya@iis.u-tokyo.ac.jp

Nobuyuki Taniguchi
Institute of Industrial Science, University of Tokyo
4-6-1 Komaba, Meguro-ku, Tokyo 153-8505, Japan
ntani@iis.u-tokyo.ac.jp

ABSTRACT

Large eddy simulation (LES) of turbulent premixed combustion flows over backward facing step been performed by using Dynamic Subgrid G-equation flamelet model. A flamelet model for the premixed flame is combined with a dynamic subgrid combustion model for the filtered propagation flame speed. The objective of study is to investigate the validity of the dynamic subgrid *G*-equation model to a complex turbulent premixed combustion for the considering of the realistic engineering application.

The calculated results were compared with experimental results and good agreement is obtained.

INTRODUCTION

Turbulent premixed flames are important because of their occurrence in spark ignition engines, and gas turbines in order to minimize NO_x formation. The challenges facing designers of combustion devices involve scale dependent unsteady dynamic behaviors that cannot be simulated well with standard ensemble or time averaged flow model, and more accurate prediction method is required. Direct numerical simulation of turbulent reacting flows places extreme demands on computational resources. At that present time, simulations can be performed only for greatly simplified reaction systems and very low Reynolds numbers. Thus there is a clear need to develop LES for reacting flows.

One of the practically relevant and better-understood types of turbulent premixed combustion is the laminar flamelet regime, in which the characteristic chemical time is much shorter than the characteristic flow time. Under this condition, combustion can be represented as the propagation of laminar flamelets, corrugated by turbulent eddies. In this study a flamelet model based on the G-equation is used. (Kerstein *et al.*, 1988) In a LES context, the G-equation is generally used to describe the filtered G field, where the propagation of the filtered-front speed is modeled. However, the filtered flame front speed is not well defined quantity and existing theoretical and empirical result for this filtered flame front speed do not agree with on another, and thus the functional form of filtered-front speed remains an open question. Recently, a dynamic subgrid model was proposed by Im *et al.* (1997) to overcome this difficulty. However, LES application using this dynamic subgrid model to a practical combustor not reported yet.

The objective of this study is to investigate the validity of the dynamic subgrid G-equation model to a complex premixed combustion flow. For the purpose of validating the LES combustion model, LESs of isothermal and reacting share layer formed at a backward facing step were carried out, and the results compared with experimental data.

MATHEMATICAL FORMULATION

LES governing equations The flow solver solves the Navier-Stokes equations that govern the conservation of mass, momentum, and energy in a fluid. The reaction solver solves the energy conservation equations and *G*-equation model. Applying a density-weighted, spatial filter to the governing equations yields the LES equation. These equations are non-dimensionalized here with respect to the inlet mean velocity U_0, the step height h, the relatively temperature $(T^*-T_u)/(T_b-T_u)$, and the thermodynamic properties at inlet. Here subscript u

means *unburned*, *b* means *burnt*. The filtering operation resulting equations can be written as:

$$\frac{\partial \bar{\rho}}{\partial t}+\frac{\partial \overline{\rho u_i}}{\partial x_i}=0 \tag{1}$$

$$\frac{\partial \overline{\rho u_i}}{\partial t}+\frac{\partial\left(\overline{\rho u_i} \tilde{u}_j\right)}{\partial x_j}=-\frac{\partial \bar{p}'}{\partial x_i}+\frac{\partial}{\partial x_j} \frac{\mu^*}{\mathrm{Re}}\left(\frac{\partial \tilde{u}_i}{\partial x_j}+\frac{\partial \tilde{u}_j}{\partial x_i}\right)-\frac{\partial \tau_{ij}^{SGS}}{\partial x_j} \tag{2}$$

$$\frac{\partial \overline{\rho T}}{\partial t}+\frac{\partial\left(\overline{\rho T} \tilde{u}_j\right)}{\partial x_j}=\frac{\partial}{\partial x_j}\left(\frac{\lambda^*}{\mathrm{Re}\,\mathrm{Pr}} \frac{\partial \tilde{T}}{\partial x_j}\right)-\frac{\partial q_j^{SGS}}{\partial x_j}+\dot{w} \tag{3}$$

$$\frac{\partial \bar{\rho} \tilde{G}}{\partial t}+\frac{\partial\left(\bar{\rho} \tilde{G} \tilde{u}_j\right)}{\partial x_j}=-\frac{\partial \gamma_j^{SGS}}{\partial x_j}+\overline{\rho_u S_L^0|\nabla G|} \tag{4}$$

Here ρ is the density, u_i is the velocity components in the x_i direction, p is the pressure, μ is the molecular viscosity, $\mu^*=\lambda^*=(T/T_u)^{0.76}$, T is the temperature, and $\dot{w}$ is the heat release from reaction. The density can be estimated directly from temperature fields; $\rho=\rho_u/(1+\tau T)$, where τ is heat release parameter, $\tau=(T_b-T_u)/T_u$. In the current formulation a low-Mach number approximation is used, eliminating acoustic waves from the model. G is a progress variable that defines the location of the flame, ρ_u is the reference reactant density, and S_L^0 is the undisturbed laminar flame speed. In the flow field, the value of G is prescribed in the range $[0,1]$. Here, G is assigned the value of zero in the unburned region and unit in the burnt region with the thin flame identified by a fixed value of $0<G_0<1$. The G-equation (4) must be solved along with the equations (1)~(3) since G is coupled with the heat release term of energy conservation equation (3) (Piana *et al.* 1996):

$$\dot{w}=\overline{\rho_u S_L^0|\nabla G|} \tag{5}$$

The unclosed subgrid terms representing respectively, the subgrid tensor, the subgrid heat flux, and the unresolved transport term are:

$$\tau_{ij}^{SGS}=\bar{\rho}\left(\widetilde{u_i u_j}-\tilde{u}_i \tilde{u}_j\right) \tag{6a}$$

$$q_j^{SGS}=\bar{\rho}\left(\widetilde{u_j T}-\tilde{u}_j \tilde{T}\right) \tag{6b}$$

$$\gamma_j^{SGS}=\bar{\rho}\left(\widetilde{u_j G}-\tilde{u}_j \tilde{G}\right) \tag{6c}$$

Dynamic subgrid model for G-equation The unresolved transport term in equation (5) is modeled using a gradient assumption (Im *et al.* 1997),

$$\gamma_k=-\bar{\rho} C_G \Delta^2|\tilde{S}| \frac{\partial \tilde{G}}{\partial x_k} \tag{7}$$

A dynamic model can be used to determine the constant C_G.

$$C_G \Delta^2=-\frac{F_i H_i}{H_j H_j} \tag{8}$$

where

$$F_k=\widetilde{\tilde{u}_k \tilde{G}}-\tilde{\tilde{u}}_k \tilde{\tilde{G}}, \quad H_k=\left(\tilde{\Delta}/\Delta\right)^2\left|\tilde{\tilde{S}}\right| \frac{\partial \tilde{\tilde{G}}}{\partial x_k}-\widetilde{|\tilde{S}| \frac{\partial \tilde{G}}{\partial x_k}}$$

$$\tilde{S}_{ij}=\frac{1}{2}\left(\frac{\partial \tilde{u}_i}{\partial x_j}+\frac{\partial \tilde{u}_j}{\partial x_i}\right), \qquad |\tilde{S}|=\left(2 \tilde{S}_{ij} \tilde{S}_{ij}\right)^{\frac{1}{2}}$$

Here $\tilde{S}_{ij}$ is the strain rate, and Δ is the characteristic length scale for smallest resolved motion; $\Delta=(\delta x_1\, \delta x_2\, \delta x_3)^{1/3}$, δx_i are the local mesh spacing. Here the $\tilde{\tilde{f}}$ denotes test filtering operated.

Modeling of the propagating term of G-equation The propagation term for filtered G-equation is approximated as,

$$\overline{\rho_u S_L^0|\nabla G|}=\bar{\rho}_u \tilde{S}_T|\nabla \tilde{G}| \tag{9}$$

where $\tilde{S}_T$ is the *filtered* turbulent flame front speed averaged over a characteristic LES cell and must be modeled.

The filtered turbulent flame speed can be obtained by using dynamic processes induced by Im *et al.* (1997). The resulting formulation can be written as:

$$\frac{\tilde{S}_T}{S_L^0}=1+C_\alpha\left(\frac{q}{S_L^0}\right)^n \tag{10}$$

$$C_\alpha=\frac{\left(S_L^0\right)^n\left[\widetilde{|\nabla \tilde{G}|}-|\nabla \tilde{\tilde{G}}|\right]}{\left[Q^n|\nabla \tilde{\tilde{G}}|-\widetilde{q^n|\nabla \tilde{\tilde{G}}|}\right]} \tag{11}$$

where n is a constant, q is the rms of the subgrid turbulent intensity, and Q is the rms of the test-grid scale turbulent intensity. They are modeled as follows. In this study, n set $n=1$.

$$q^2=\widetilde{u_i u_i}-\tilde{u}_i \tilde{u}_i, \quad Q^2=\tilde{\tilde{u}}_i \tilde{\tilde{u}}_i-\tilde{\tilde{u}}_i \tilde{\tilde{u}}_i \tag{12}$$

PROBLEM CONFIGURATION

The experiments conducted by Pitz et al. (1983) were carried out in the two-dimensional combustor apparatus. The geometry of the computational domain used in the calculations is shown in figure 1. The x, y and z directions will be referred to as the streamwise, normal and spanwise directions, respectively. All lengths are normalized by the step height, h $(=0.0254\ m)$. Flow is from left to right. The reacting and nonreacting flowfield is simulated for entrance Reynolds number $Re_h=22,100$ where the Reynolds number $Re_h=U_0 h/\nu$, is based on step height

h, averaging inlet velocity U_0, and kinematic viscosity v. The mean velocity, pressure and temperature at the inlet are $U_0 = 13.3$ *m/s*, $p_0 = 1$ *atm* and $T_0 = 293$ *K*, respectively. The reacting case is a premixed propane-air flame with an equivalence ratio of Φ=0.57, the laminar flame speed $S^0_L = 0.127$ *m/s* at corresponding conditions, stabilized in a turbulent free shear layer formed at a backward facing step.

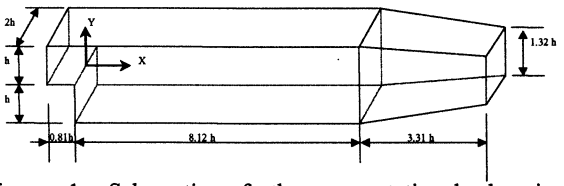

Figure 1: Schematic of the computational domain (h=0.0254 m)

NUMERICAL METHOD

The governing equation equations are discretized on a staggered mesh by finite volume technique. Second order schemes are used in space and time, central differencing for convection and diffusion terms and Adams-Bashforth schemes in time. For numerical stability, however, QUICK scheme is used convection terms of the G-equation and the energy conservation equation. All simulation starts from rest and unsteady flow characteristics evolve naturally. The simulations are conducted using a nonuniform grid resolution of 251×52×20 grid points (261,040 cells) in the streamwise, normal and spanwise directions, respectively. The Size of grid are by given $\Delta x=\Delta z=0.05h$, $\Delta y=0.022\sim0.005h$, and minimum wall unit is $y^+_{min}=9.9$ at near the wall, where wall unit is defined as $y^+=u_\tau y/v$, y is a distance from the wall and u_τ is a wall friction velocity.

No-slip wall condition is used along solid walls that include top and bottom wall boundary, as well as the step-wall boundary. Wall function by Spalding's law is, however, used along solid walls at the converging exit region. The flow is assumed to be homogenous in the spanwise direction justifying the use of periodic boundary conditions. The inlet velocity is obtained from the experimentally measured mean profile, on which "white noise" of 4%, 2% and 2% is superimposed in the streamwise, spanwise and normal directions respectively. A convective boundary condition is used at the outlet.

To decouple the pressure-velocity system, a Poisson equation, derived from discretized versions of the continuity and momentum equations, is constructed for the pressure. In order to solve for velocity $\overline{u}_i$ and pressure $\overline{p}'$, equation (2) is written as

$$\frac{\partial\overline{\rho}\widetilde{u}_i}{\partial t} = -\frac{\partial\overline{p}'}{\partial x_i} - \frac{\partial\left(\overline{\rho}\widetilde{u}_i\widetilde{u}_j\right)}{\partial x_j} + \frac{\partial}{\partial x_j}\frac{\mu^*}{\mathrm{Re}}\left(\frac{\partial\widetilde{u}_i}{\partial x_j}+\frac{\partial\widetilde{u}_j}{\partial x_i}\right) - \frac{\partial\tau_{ij}^{SGS}}{\partial x_j} \equiv -\frac{\partial\overline{p}'}{\partial x_i} + B_i \quad (13)$$

Integrating this equation from t to $t+\Delta t$ gives, approximating the integral over B_i,

$$(\overline{\rho}\widetilde{u}_i)^{n+1} = (\overline{\rho}\widetilde{u}_i)^n - \Delta t\frac{\partial\overline{p}'}{\partial x_i} + \Delta t\left\{\frac{3}{2}B_i^n - \frac{1}{2}B_i^{n-1}\right\} \quad (14)$$

A Poisson equation is obtained by taking the divergence of equation (14) giving

$$\frac{\partial^2\overline{p}'}{\partial x_i^2} = -\frac{1}{\Delta}\left\{\frac{\partial}{\partial x_i}(\overline{\rho}\widetilde{u}_i)^{n+1} - \frac{\partial}{\partial x_i}(\overline{\rho}\widetilde{u}_i)^n\right\} + \frac{\partial}{\partial x_i}\left\{\frac{3}{2}B_i^n - \frac{1}{2}B_i^{n-1}\right\} \quad (15)$$

An estimation of $\partial(\overline{\rho}\widetilde{u}_i)^{n+1}/\partial x_i$ is needed. It is at this point that the conservation of mass, equation (1), is utilized. It gives, at the time-step n+1,

$$\frac{\partial}{\partial x_i}(\overline{\rho}\widetilde{u}_i)^{n+1} = -\left(\frac{\partial\overline{\rho}}{\partial t}\right)^{n+1}. \quad (16)$$

With $\overline{\rho}^{n+1}$ already known from solving G-equation (4), we can use a backwards difference to estimate $(\partial\overline{\rho}/\partial t)^{n+1}$. For example, based upon time steps, n and n+1,

$$\frac{\partial}{\partial x_i}(\overline{\rho}\widetilde{u}_i)^{n+1} = -\left(\frac{\partial\overline{\rho}}{\partial t}\right)^{n+1} \quad (17)$$

Therefore pressure $\overline{p}'$ is obtained by solving equation (15). (McMurtry1986, Lesieur, M. 1993)

RESULTS AND DISCUSSION

Isothermal flow simulation In order to conform the predictive capabilities of LES code for incompressible and isothermal flows, LES of turbulent flow over backward-facing step is carried out at $Re_h=22,100$. The flow can be separated into the mixing layer region, comprising of the curved shear-layer flow from the initial boundary layer at separation to the reattachment point and the relaxation region, from the reattachment point to full recovery of the turbulent boundary layer.

Figure 3 shows an instantaneous representation of the iso surface $\overline{u}=0$ separating the shear layer from the recirculation region, and contours of the spanwise vorticity $\overline{\omega}_z$ at the center-plane for the non-reacting flow. Development of the vortices in the mixing layer is quite clear and they appear similar to the vortices of the reacting flow of figure 4.

The layer curves down towards the lower wall and impinges on the wall at the reattachment point. The size of the recirculation bubble depends on to a large

extent on the rate of growth of the reattaching shear layer into the recirculation zone, see time averaged streamwise velocity profiles in figure 8.

As in mixing layers, the topological structure of the reattaching shear layer is determined by the development of large-scale coherent structure formed by the Kelvin-Helmhotz instability in the shear layer figure 3. The resulting structures are predominantly two-dimensional and grow by fluid entrainment and coalescence. The growth of these structures affects the recirculation zone as well as the rate of spread of the upper boundary of the shear layer into the free-stream.

Figure 8 and 9 show time averaged profiles of streamwise velocity components and its rms fluctuations for non-reacting flow. The statistical quantities averaged over $0.07sec$ during the premixed gas passed 3 times through the test combustor rig. LES results show good agreement with the experiment for both the streamwise velocity and its rms fluctuations. LES satisfactorily predicts the time-averaged length of the recirculation region $x_R/h = 6.8$ compared with the experiment value of 7.0. (For the experiment, it is reported that velocity profiles are taken in increments of h near the reattachment point making the values accurate to $\pm 0.5h$.)

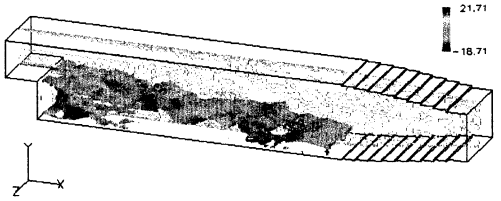

Figure 3: Instantaneous representation of the non-reacting flow (Φ=0) in terms of the iso surface $\overline{U} = 0$ separating the shear layer from the recirculation region, and contours of the spanwise vorticity $\overline{\omega}_z$ at the centerplane.

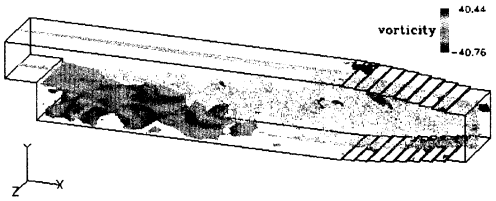

Figure 4: Instantaneous representation of the reacting flow (Φ=0.57) in terms of the iso surface $\overline{U} = 0$ separating the shear layer from the recirculation region, and contours of the spanwise vorticity $\overline{\omega}_z$ at the center-plane

Reacting flow simulation

In order to validate the dynamic subgrid combustion model, LES of turbulent premixed combustion flow is performed at Re_h=22,100, corresponding to the experiments by Pits (1983).

Figure 4 shows instantaneous iso-velocity surface $u=0$ separating the shear layer from the recirculation region and contours of the spanwise vorticity $\overline{\omega}_z$ at the center-plane for the reacting flow (Φ=0.57). The vortices move with nearly the same convective velocity ay each point in space and with a general trend of increasing velocities as they move downstream. Because this is a reacting flow with energy release and expansion, the observed acceleration is expected. Nonreacting flows behave similarly but with less acceleration of the vortices. There is close resemblance in the development of eddies in the reacting and nonreacting shear layers under investigation. Because of the increase in viscosity with reaction, there is an order of magnitude reduction in Reynolds number. There is a reduction in small-scale turbulence due to heat release in the mixing layer.

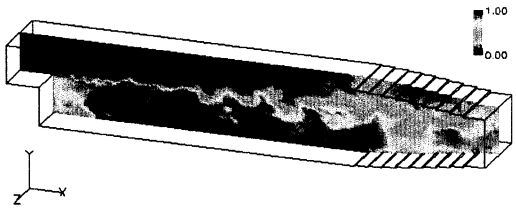

Figure 5: Instantaneous normalized temperature distribution at the center-plane for the reacting flow (Φ=0.57).

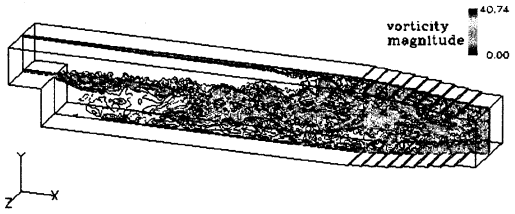

Figure 6: The instantaneous vorticity magnitude distribution at the center-plane for the reacting flow (Φ=0.57).

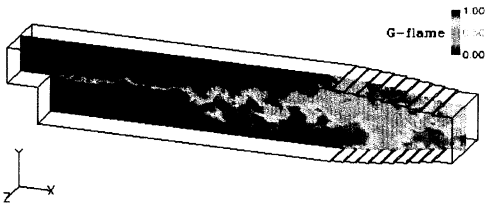

Figure 7: The instantaneous flame (G-field) distribution at the center-plane for the reacting flow (Φ=0.57).

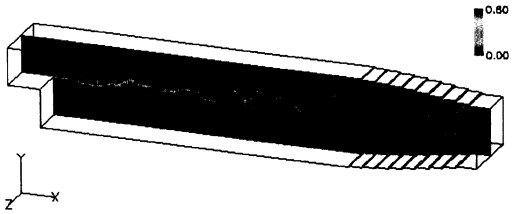

Figure 8: The instantaneous effective reaction rate distribution $\varpi = \bar{\rho}_u \tilde{S}_T |\nabla \tilde{G}|$ at the center-plane for the reacting flow (Φ=0.57).

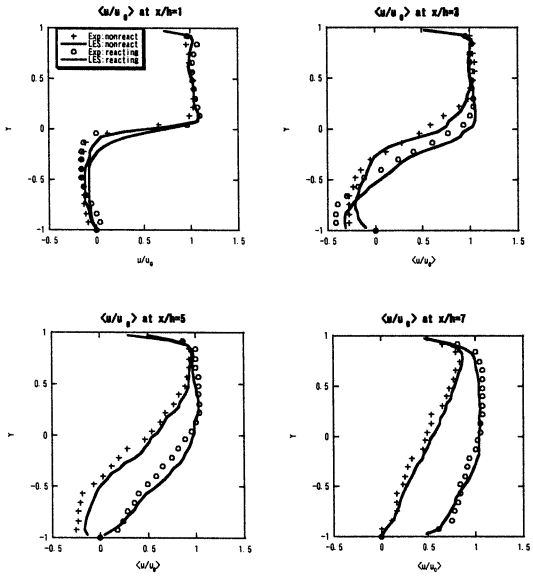

Figure 8: Time averaged streamwise velocity component profiles for the non-reacting and reacting flows (a) x/h = 1 (b) x/h = 3 (c) x/h = 5 (d) x/h = 7

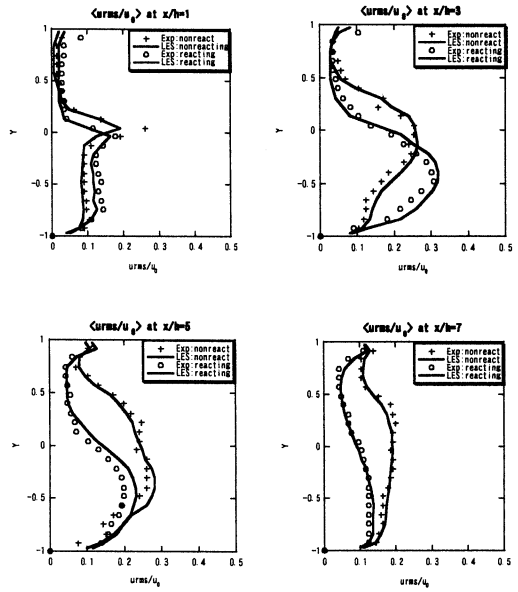

Figure 9: Time averaged streamwise u-rms velocity fluctuation profiles for the non-reacting and reacting flows (a) x/h = 1 (b) x/h = 3 (c) x/h = 5 (d) x/h = 7

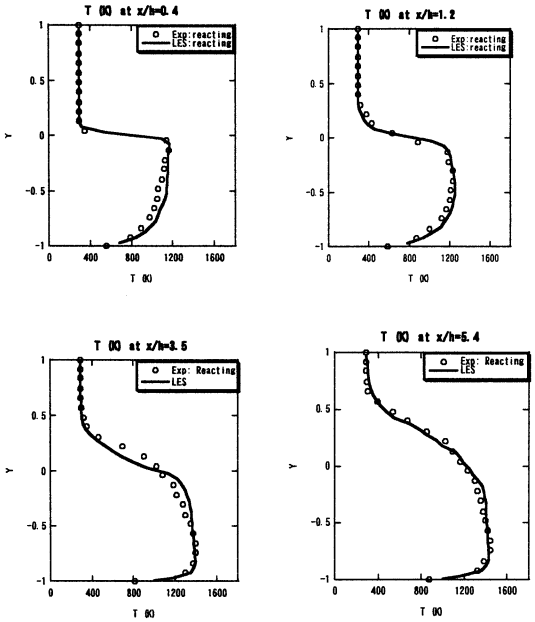

Figure 10: Time averaged temperature profiles for the reacting flow (a) x/h = 0.4 (b) x/h = 1.2 (c) x/h = 3.5 (d) x/h = 5.4

Figure 5 shows the instantaneous normalized temperature distribution at the center-plane. Figure 6 shows the instantaneous vorticity magnitude distribution at the center-plane. LES is successful in capturing the global flow features, in particular the shape of initial shear layer and the downstream evolution of the large scale structure.

Figure 7 shows the instantaneous flame (G-field) distribution. In the reaction case the incoming fluid contains cold premixed reactants (293*K*), which mix with hot combustion products in the initial shear layer behind the step prior to burning. Figure 8 shows the instantaneous effective reaction rate distribution $\varpi = \bar{\rho}_u \tilde{S}_T |\nabla \tilde{G}|$. Heat releases occur mainly in the large-scale structures that form early in the shear layer as they entrain cold reactants and hot products.

Figure 8 and 9 show time averaged profiles of streamwise velocity components and its rms fluctuations. For reaction case the LES profiles are in reasonable agreement with the experimental data. The length of the recirculation zone is found to be shorter in the reacting case, and the maximum reverse velocity is higher due to gas expansion. The LES combustion model is successful in predicting these features; the maximum reverse velocity is 0.42 U_0 (0.44 U_0) while the length of the recirculation region is x_R/h = *4.4* (4.5) (the experimental value given in braces). It can be observed that the turbulent intensity is well predicted by LES both in the non-reacting and reacting case in figure 9. For both flows, regions of high turbulence occur in the shear layer and broaden with downstream distance from the step.

Figure 10 shows time averaged temperature profiles for the reacting. The averaged temperature profiles show good agreement between LES and experimental data.

For a better understanding of the process of development of flame propagation, a sequential series of snapshots of the flame from the simulation are presented in figure 11. Calculation for combustion flow is started from fully developed nonreacting turbulent flow. Ignition was given that G=1 at the backward facing step wall and G=0 at the other region as an initial combustion condition in figure 11(a). Time interval between presented results is 9.3 ms for during 0.07 sec from figure 11(a) to (h) and the premixed gas passed 3 times through the test combustor rig at that time. Development of the vortices in the initial stages of the mixing layer is quite clear and they appear similar to the vortices of the reacting flow. As for the reacting flow, the process of coalescence of eddies can be seen. These observations suggested that heat release which results in expansion and increase in kinematic viscosity of gas mixture in the mixing layer does not considerably affect the vortex shedding behind the step.

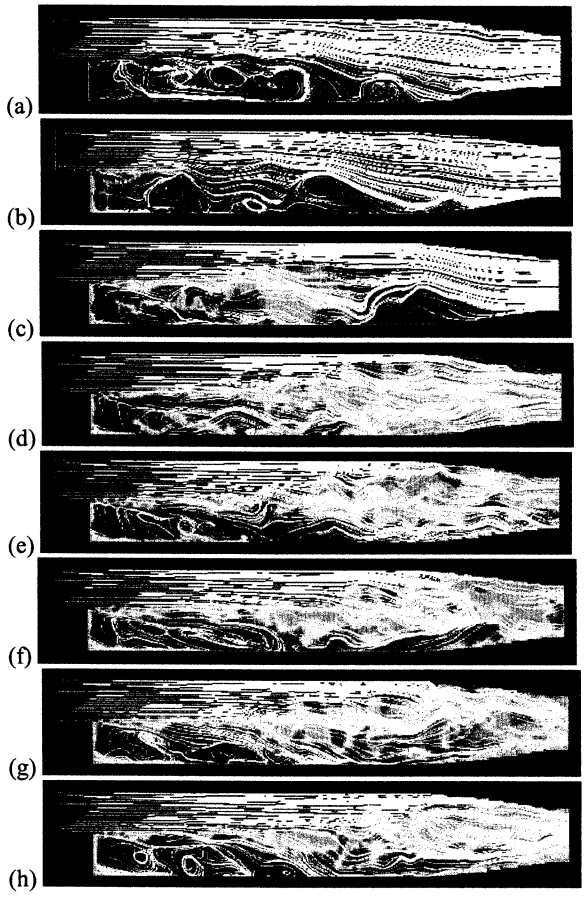

Figure 11: Sequential series of instantaneous temperature and streamline from LES of flame; time interval between is 9.3 ms for during 0.07 s from (a) to (h) and the premixed gas passed 3 times through the test combustor rig.

CONCLUSION

In order to investigate the validity of the dynamic subgrid G-equation combustion, LES of turbulent premixed flames over backward facing step was carried out at Re_h=22,100, corresponding to the experiments of Pitz *et al.* (1983).

LES of incompressible isothermal flow was also performed to conform the predictive capabilities of LES code.The dynamic Smagorinsky SGS model is employed in reacting and non-reacting flow study.

LES of the validation case with the dynamic subgrid combustion model yields good overall agreement with the experimental data. LES is successful in capturing the global flow features, in particular the shape of the initial shear layer and the downstream evolution of large scale structures.

The simulations show that LES of turbulent premixed flames with *G-equation* flamelet model is of practical use for practical engineering application. The validity of the dynamic subgrid G-equation combustion model was confirmed.

References

Im, H. G. and Lund, T. S.,1997 "Large eddy simulation of turbulent front propagation with dynamic subgrid models", *Phys. Fluids* 9 (12), pp.3826-3833

Germano, M., Piomelli, U., Moin, P. and Cabot, W. H., 1991, "A dynamic subgrid-scale eddy viscosity model", *Phys. Fluids* A 3, pp.1760.

Kerstein, A.R., Ashurst, Wm. T. and Williams, F.A., 1988, "Field equation for interface propagation in an unsteady homogeous flow field", Phys. Rev. A. 37, 2728

Lesieur, M., Comte, P., Les Houches 1993, Session LVIX, Course 5, NATO ASI, pp. 221-255.

McMurtry, P. A., Jou, W. H., Riley, J. J., Metcalfe, R. W., *AIAA J.* (1986), 24, pp. 962-970.

Menon, S., 1996, "Large-eddy simulation of combustion instabilities", In proceedings of the Sixth International Conference on Numerical Combustion. New Orleans, Louisiana, March 4-6

Piana, J., Veynante, D., Candel, S., and Poinsot, T., 1996, In Proceedings of the Second ERCOFAC Workshop on Direct and Large-Eddy Simulation, Grenoble.

Pitz, R.W. and Daily, J.W., 1983, "Combustion in a Turbulent Mixing Layer formed at a rearward-Facing Step", *AIAA. J.*, 21(11): 1565-1570